Available online at www.sciencedirect.com
SCIENCE DIRECT®
Journal of Solid State Chemistry 177 (2004) 4732–4742
JOURNAL OF SOLID STATE CHEMISTRY
http://elsevier.com/locate/jssc

Kinetic ordering of atoms in sodium chlorate–bromate solid solutions

A.G. Shtukenberg,[a,*] I.V. Rozhdestvenskaya,[a] D.Yu. Popov,[b] and Yu.O. Punin[a]

[a] *Crystallography Department, St.-Petersburg State University, Universitetskaya emb., 7/9, 199034,, St.-Petersburg, Russia*
[b] *Institute of Chemistry FEBRAS, Vladivostok, Russia*

Received 27 January 2004; received in revised form 27 May 2004; accepted 27 May 2004

Abstract

Kinetic ordering of anions in $Na((ClO_3)_{1-x}(BrO_3)_x)$ solid solutions with anomalous birefringence was studied by means of single crystal X-ray diffraction. The crystal structures of the two samples ($x = 0.10$ and 0.255) cut out from the {100} growth sectors were refined in the ideal space group $P2_13$ and in two of its subgroups—monoclinic $P2_1$ and triclinic $P1$ with $R = 0.030-0.038$. The final choice of monoclinic symmetry was confirmed by the analysis of the diffraction pattern and Cl/Br distribution over the halogen crystallographic sites. The Cl/Br ordering reflects the geometrical difference of these sites with respect to the growth front orientation. The observed optical indicatrix was successfully reproduced in the point-dipole approximation. According to our data and the data of Crundwell et al. (Acta Crystallogr. Sect. B 53 (1997) 189), the degree of ordering increases in the middle of the isomorphous series along with the birefringence. The obtained results confirm the hypothesis of growth dissymmetrization.
© 2004 Elsevier Inc. All rights reserved.

Keywords: Kinetic phase transition; Sodium chlorate; Sodium bromate; Dissymmetrization; Solid solution; Optical anomalies

1. Introduction

Apart from the equilibrium orde–disorder phase transitions occurring in crystals of solid solutions there is a wide class of kinetic order–disorder phase transitions. The principal difference between these classes appears in the parameters, which govern the phase transformation. The temperature, pressure, magnetic field or any other thermodynamic parameters control equilibrium phase transitions. On the contrary, the kinetic phase transitions are guided by the kinetic factors such as crystal growth rate and/or structure of the growing surface. This class looks rather exotic, but nevertheless, it is typical for the solution grown mixed crystals. Examination of these phase transitions is of great importance, since it gives a new insight into the crystal growth processes.

There are kinetic transitions (see above) of opposite character, namely, ordering and disordering. In this paper we consider the kinetic ordering phenomenon (the so-called ''growth ordering of atoms'' or ''growth dissymmetrization''), which is usually accompanied by optical anomalies (i.e., some distortions of the ideal optical indicatrix) and can be described in the following way. The positions of the atoms, which are strictly equivalent in the bulk of a crystal, are non-equivalent geometrically and energetically in the surface of the growing crystal. This gives rise to the ordered distribution of isomorphous atoms in the surface layer. The ordered state at the surface is then buried in the bulk of the crystal during its growth. The state is metastable but it can be retained in the crystal for a long time due to very low diffusion rates in solids. Kinetic ordering was discovered and studied in at least 20 compounds, e.g. in quartz [1], alums [2,3], garnets [4,5], topaz [6], $Na_2Cd(SO_4)_2{\cdot}H_2O$ [7], etc. Unfortunately, *different* aspects of the phenomenon were studied for *different* compounds that led to some ambiguity in the data interpretation. For example, ordering of the trivalent cations in ugrandite garnets and related optical anomalies were studied in detail [4,5,8,9], however, reliable data on the effect of crystal composition and growth conditions are still unavailable. On the contrary, these growth aspects were examined for the alum crystals, but the structural reasons for the anomalous birefringence

*Corresponding author.
E-mail address: sasha@as3607.spb.edu (A.G. Shtukenberg).

0022-4596/$ - see front matter © 2004 Elsevier Inc. All rights reserved.
doi:10.1016/j.jssc.2004.05.063

remains unclear so far [2,3,10]. The main objective of the present paper is to demonstrate all the principal aspects of the growth dissymmetrzation phenomenon for *one and the same* object. It should bring a more persuasive character to the hypothesis of kinetic ordering and help in its further development. Additionally, the paper is aimed to collect some new data on the growth ordering phenomenon and the crystal structures of solid solutions.

The mixed crystals of sodium chlorate—bromate $Na(ClO_3,BrO_3)$, which can easily be grown from low-temperature aqueous solutions under well-controlled conditions, were chosen for the study. Their ideal crystal structure and physical properties are well known. Unlike the end members of the series, the solid solutions reveal strong anomalous birefringence that is inconsistent with the ideal cubic space group $P2_13$. According to the recent studies [11,12], the birefringence is likely to be induced by the anion growth ordering. However, the authors failed to associate the Cl/Br ordering either with the unit cell distortions, mechanism of growth dissymmetrization, or anomalous birefringence. Therefore, the choice of $Na(ClO_3,BrO_3)$ solid solutions seems to be appropriate.

2. Experimental

The method of temperature lowering was used for growing mixed crystals of $Na((ClO_3)_{1-x}(BrO_3)_x)$ from aqueous solutions at the temperatures $T = 30-35°C$ and the relative supersaturations 2–9%. The crystal size varied from 1 mm up to 2–3 cm. The crystals with $x < 0.8$ were shaped only by the {100} faces. Other mixed crystals exhibited predominance of the {100} faces with the minor contribution of the two tetrahedra {111} and $\{\bar{1}\bar{1}\bar{1}\}$. The pure sodium bromate crystals were shaped only by the tetrahedra. The anomalous birefringence in the {100} growth sectors was measured with a Berek compensator using the 1–3 mm thick sections parallel to {100} and {110}. Considering the linear dependence of the refractive index ($n_{NaClO_3} = 1.515$ and $n_{NaBrO_3} = 1.594$ [13]) on the composition, the BrO_3 content was determined within an accuracy of 3 mol% with the oil immersion method.

The three samples H1, H2 and H2a were cut out from the {100} growth sectors of the crystals. The growth faces of the two plate-like samples H1 and H2a normal to the sample holder were taken as (010). The sample H2 was shaped to a sphere using a compressed air grinder. This enabled the accurate comparison of the symmetrically equivalent reflections but made an indexing of the growth front direction impossible.

The diffraction data were collected by a ω -scanning in a four-circle X-ray autodiffractometer Nikolet-P3/R3 (Mo$K\alpha$ radiation, graphite monochromator) in a half of the reciprocal space (sample H1) or the whole reciprocal space (sample H2), see Table 1 for the experimental details. The measured intensities were then corrected for the long-term fluctuations of the incident beam and the *LP*-factor. The refinements of the crystal structures were performed with the CSD program package [14]. The atomic scattering factors f were taken from the *International Tables for X-ray Crystallography* [15]. The temperature factors were refined in the anisotropic approximation. The halogen sites occupancies were refined separately using the set of reflections with $\sin\Theta/\lambda < 0.5$.

Table 1
Samples and X-ray diffraction experiment

Sample	H1	H2
Composition, $x = Br/(Br + Cl)$	0.10	0.255
$n_\gamma - n_\alpha$	0.0007(1)	0.0010(1)
Crystal size, mm	$0.25 \times 0.25 \times 0.30$	Sphere, $r =$ 0.11
μ, cm^{-1}	26.40	47.44
ρ_{calc}, g/cm^3	2.572(1)	2.708(1)
Z	4	4
$(\sin\Theta/\lambda)_{max}$	0.992	0.995
Number of measured reflections	3867	9516
a (Å)	6.590(1)	6.611(1)
b (Å)	6.591(1)	6.610(1)
c (Å)	6.592(1)	6.611(1)
α (deg)	90.00(1)	89.99(1)
β (deg)	90.06(1)	90.06(1)
γ (deg)	90.00(1)	90.01(1)
$\langle a \rangle$ (Å)	6.591	6.611
Refinement in the space group $P2_13$		
Number of unique reflections, $F > 4\sigma_F$	388	421
Number of free parameters	18	18
R	0.032	0.030
R_w	0.037	0.038
R_m	0.074	0.087
Refinement in the space group $P2_1$		
Number of unique reflections, $F > 4\sigma_F$	1835	2139
Number of free parameters	91	91
R	0.034	0.036
R_w	0.036	0.037
R_m	0.032	0.065
Refinement in the space group P1		
Number of unique reflections, $F > 4\sigma_F$	3313	3842
Number of free parameters	182	182
R	0.035	0.038
R_w	0.037	0.040
R_m	0.073	0.054

$R = \sum|F_o - F_c|/\sum|F_o|$; $R_w = \sum w|F_o - F_c|/\sum|F_o|$; weight scheme $w = 1/(\sigma F^2 + kF_o^2)$, $k = 0.001-0.002$; $R_m = \sum|F_{av.}^2 - F_i^2|/\sum F_i^2$, $F_{av.}$—is the average of the set of observed symmetry related structure factors and F_i is the ith individual observed structure factor for that set.

The optical indicatrix was calculated in the point-dipole approximation [16–18] using the software designed by D.Yu. Popov. The input data included the lattice constants, the atomic coordinates, and the electronic polarizabilities of atoms (α). The electronic polarizabilities of Na^{+}, Cl^{5+}, Br^{5+} and O^{2-} were taken from [19]. The polarizability of O^{2-} ($\alpha_O = 1.52\,Å^3$) was additionally refined for the $NaClO_3$ and $NaBrO_3$ cubic structures [20,21] by fitting the calculated refractive index to the experimentally measured value [13]. The polarizabilities of O^{2-} in the solid solutions were found using the additivity rule. The final set of polarizabilities was as follows: $\alpha_{Na} = 0.32\,Å^3$, $\alpha_{Cl} = 0.32\,Å^3$, $\alpha_{Br} = 0.8\,Å^3$, $\alpha_{O(chlorate)} = 1.36\,Å^3$ and $\alpha_{O(bromate)} = 1.42\,Å^3$. Changes in these values have no significant influence on the optical indicatrix orientation, but affect the birefringence. This fact is in agreement with the calculations performed for other compounds [5,17].

3. Results

3.1. Optical indicatrix

The crystals of the end members do not display optical anisotropy, whereas the solid solutions show anomalous birefringence. The optical indicatrix of the {100} growth sectors is a biaxial ellipsoid with n_β directed normal to the growth face, and n_α and n_γ going along diagonals of the faces. For instance, n_β||[010], n_α ||[101] and n_γ ||[10$\bar{1}$] for the (010) growth face (Fig. 1).

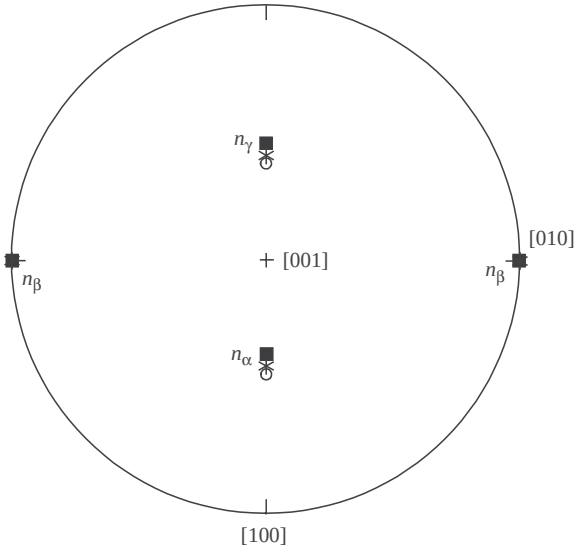

Fig. 1. Stereographic projection of the optical indicatrix of the $Na(ClO_3,BrO_3)$ solid solutions. Open circles and solid squares correspond to the samples H1 and H2, respectively. The observed optical indicatrix for both the samples is shown with the stars. The vector [010] represents a normal to the growth face.

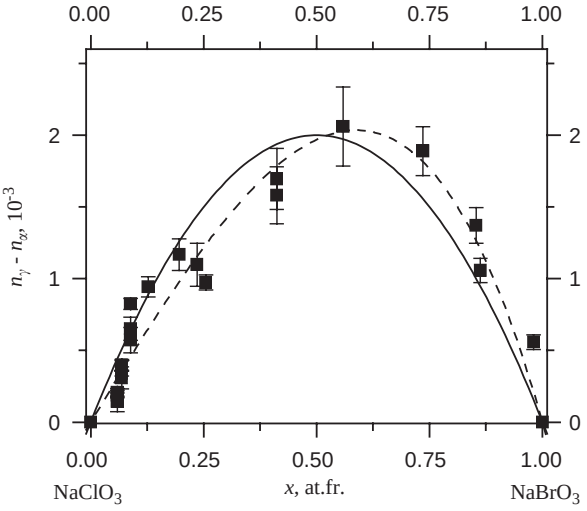

Fig. 2. The value of anomalous birefringence as a function of the crystal composition. Solid line—approximation by a parabola, dashed line—fitting with Eq. (4) with the variable distribution coefficient calculated from Eq. (5).

The crystals are nearly optically neutral, i.e. the axial angles $2V \approx 90°$ and $n_\gamma - n_\beta \approx n_\beta - n_\alpha$. It means that the maximal birefingence $n_\gamma - n_\alpha$ is observed in the sections parallel to the growth face (010), and both the (100) and (001) sections are optically isotropic. Orientation of the optical indicatrix was found to agree with the data obtained by Gopalan et al. [11] and Crundwell et al. [12] and to be consistent with the monoclinic (or lower, triclinic) symmetry. The birefringence $n_\gamma - n_\alpha$ varies from 0 in the end members up to 0.002 in the middle of the series (Fig. 2). The maximum value of the birefringence reported for the {100} growth sectors [12] was 0.0036 for the chlorine-rich crystals.

The cubic symmetry suggests an isometric crystal habit, however, some lamellar or needle-shaped crystals occur. The morphological anisotropy seems to originate from the difference in the dislocation densities and dislocation structures of the different {100} growth pyramids [22,23]. This means that these growth sectors grew under the same conditions but their normal growth rates differed significantly. It has been found for two lamellar crystals that the variations of growth rates by 22–24 times caused changes in the value of anomalous birefringence of not more than 40%.

3.2. Analysis of diffraction pattern

Growth dissymmetrization usually causes only slight distortions of the unit cell and of the atomic structure. Therefore, certain difficulties may arise in determination of the true symmetry and in the refinement of crystal structure. To obtain reliable structural information it is necessary to analyze the diffraction pattern in detail and refine the crystal structure in a number of space groups. The final choice of the space group is based on (1) the

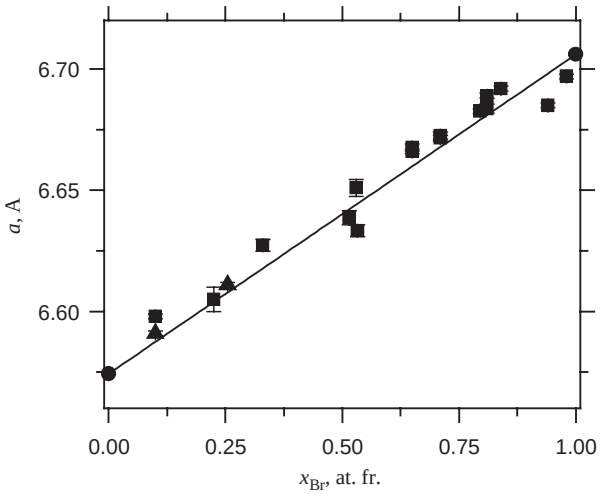

Fig. 3. Averaged (cubic) lattice constant as a function of the crystal composition. Triangles—our data, squares—data from [12], straight line connects the values for the end members [20,21]. The error bars were usually smaller than the point size.

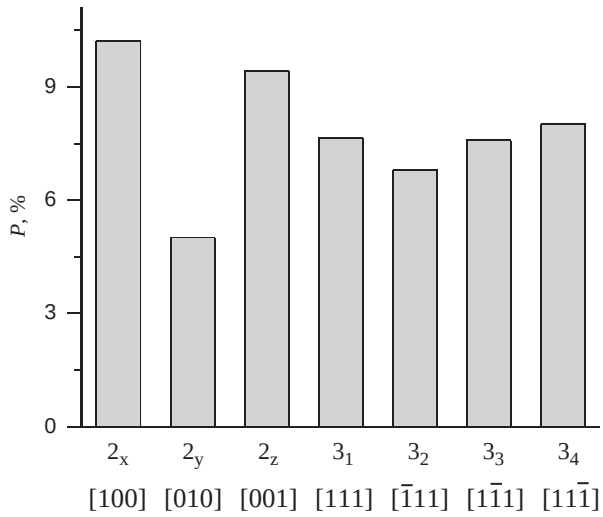

Fig. 4. Relative number of groups of reflections (P) breaking the indicated symmetry operations. Sample H2.

unit cell dimensions; (2) the intensities of reflections, which are equivalent under symmetry operations; (3) the reflection conditions; (4) the residual factors calculated for the refinements in different space groups, and (5) the site occupancies, bond lengths and angles. As it has been found for grossular-uvarovite [4] and grossular-andradite garnets (our unpublished data), these are highly desirable to prove the dissymmetrization (of any nature) and to recognize the true crystal symmetry. The average cubic lattice constants determined in our experiments agree well with the available data [12] and follow the Vegard's law (Fig. 3). The cubic unit cell of $Na((ClO_3)_{1-x}(BrO_3)_x)$ solid solutions is slightly distorted (Table 1, [12]). Only the lattice angle β deviates significantly from 90° that restrict the possible crystal symmetry to the orthorhombic, monoclinic or triclinic system. The orthorhombic coordinate axes should coincide with the two-fold axes and be parallel to the cube edges $\langle 100 \rangle$. Respectively, the principal axes of the optical indicatrix should also go along these directions. Since n_γ and n_α go along the diagonals of the cubic face, the orthorhombic system contradicts the optical data. The indexing of both the oriented samples H1 and H2a showed that the growth face corresponded to the (010) plane, and the crystal symmetry could be either monoclinic or triclinic. Crundwell et al. [12] reported *quite similar* unit cell distortions for the same compound, but the [010] axis was found to *lie in the plane* of the growth face. This principal difference is not clear yet.

The intensities of the equivalent reflections were compared for the spherical sample H2. The reflections, which were equivalent relative to a certain symmetry operation, were grouped, and each group was analyzed separately. If the difference in the intensities $I_{max} - I_{min}$ within a group exceeded a certain threshold value, the group was assumed to violate the symmetry operation. A set of the intensity e.s.d.'s or the differences in the intensities within the Friedel pairs was used as the threshold criterion. The results appeared to be similar for the different criteria (see, for example, the histogram (Fig. 4) plotted for the criterion $I_{max} - I_{min} > 2(I_{hkl} - I_{\overline{hkl}})$). It is clearly seen that all the symmetry operations are broken. The three-fold axes are absent in 6.80-8.01% of groups of reflections, whereas the parts of violations P found for the different two-fold axes vary in a wide range. The [010] axis is violated about two times fewer than the two other axes [100] and [001] (5.01% in comparison with 9.41% and 10.22%, respectively). The analysis confirms the reduction of symmetry down to the Laue class 1 (all the symmetry operations are violated) or at least to the Laue class $2/m$ (the two-fold axis [010] remains inviolate).

Only a few weak reflections with $I > 4\sigma_I$ were found, which are forbidden in the cubic space group $P2_13$. They violate two of the three two-fold screw axes, while the 2_1 axis parallel to the [010] remains inviolate. Any certain conclusion on the true symmetry cannot be made from the very low number of forbidden reflections; however, the monoclinic space group $P12_11$ is favorable.

Thus, the possible crystal symmetry is limited to either the monoclinic space group $P12_11$ or the triclinic space group $P1$.

3.3. Crystal structure

The crystal structures were refined in the following three space groups: $P2_13$, $P2_1$ and $P1$. The atomic coordinates, temperature factors and site occupancies are listed in the Tables 2–4. Unfortunately, due to the strong pseudo-symmetry, R-factors are useless for the

Table 2
Atomic coordinates, temperature factors and site occupancies for the samples H1 (upper line) and H2 (lower line); space group $P2_13$

Site	Occupancy	x	y	z	$U_{eq} \times 100$ (Å^2)
Hal	$Cl_{0.900(7)}Br_{0.100(7)}$	0.41610(5)	x	x	1.583(8)
	$Cl_{0.747(6)}Br_{0.253(6)}$	0.41393(6)	x	x	1.610(6)
Na	1	0.0694(1)	x	x	2.38(2)
	1	0.0703(2)	x	x	2.23(2)
O	1	0.3022(3)	0.5928(2)	0.5054(3)	2.67(4)
	1	0.3006(3)	0.5949(3)	0.5051(3)	2.50(5)

$U_{eq} = 1/3[U_{11}a^{*2}a^2 + \ldots 2U_{23}b^*c^*bc\cos\alpha]$.

Table 3
Atomic coordinates, temperature factors and site occupancies for the samples H1 (upper line) and H2 (lower line); space group $P2_1$

Site	Occupancy	x	y	z	$U_{eq} \times 100$ (Å^2)
Hal1	$Cl_{0.865(2)}Br_{0.135(2)}$	0.58457(6)	0.91590	0.33453(6)	1.599(8)
	$Cl_{0.703(5)}Br_{0.297(5)}$	0.58669(5)	0.91590	0.33656(5)	1.597(8)
Hal2	$Cl_{0.932(2)}Br_{0.068(2)}$	0.08317(6)	0.58325(8)	0.16667(6)	1.564(9)
	$Cl_{0.784(5)}Br_{0.216(5)}$	0.08526(6)	0.58823(8)	0.16468(6)	1.584(8)
Na1	1	0.4307(2)	0.9294(2)	0.8197(2)	2.36(3)
	1	0.4296(2)	0.9346(3)	0.8209(2)	2.24(3)
Na2	1	0.9308(2)	0.5680(2)	0.6810(2)	2.40(3)
	1	0.9299(2)	0.5755(3)	0.6799(2)	2.28(3)
O1	1	0.8029(3)	0.9064(4)	0.7443(3)	2.59(4)
	1	0.8007(3)	0.9124(4)	0.7447(3)	2.55(5)
O2	1	0.3015(3)	0.5927(3)	0.7540(3)	2.59(4)
	1	0.2999(3)	0.5991(4)	0.7547(3)	2.47(5)
O3	1	0.4951(3)	0.8004(4)	0.1573(3)	2.59(5)
	1	0.4955(4)	0.8053(4)	0.1563(3)	2.50(5)
O4	1	0.9950(3)	0.6957(4)	0.3422(3)	2.64(5)
	1	0.9946(4)	0.7040(4)	0.3431(3)	2.47(5)
O5	1	0.5927(3)	0.5039(4)	0.5515(3)	2.66(5)
	1	0.5938(3)	0.5107(4)	0.5500(3)	2.49(5)
O6	1	0.9075(3)	0.4937(4)	0.0527(3)	2.63(5)
	1	0.9064(3)	0.5009(4)	0.0502(4)	2.48(5)

$U_{eq} = 1/3[U_{11}a^{*2}a^2 + \cdots 2U_{23}b^*c^*bc\cos\alpha]$.

space group determination. They continually increase as the crystal symmetry reduces varying from 0.030 to 0.038 (Table 1) and leaving the smallest values to the refinements in the cubic space group. This is caused by the large correlation of matrix elements in monoclinic and triclinic space groups.

The final choice of the space group can be based on the analysis of the Cl/Br distribution over the halogen sites. A single halogen site in the cubic space group $P2_13$ is split into two different sites in the monoclinic space group $P2_1$ and into four different sites in the triclinic space group $P1$. The four different triclinic occupancies are grouped into two pairs. The differences within each pair are comparable with the experimental errors and are significantly smaller than the differences between the pairs (Table 4). Correctness of the occupancies is also confirmed by the proportionality of the average halogen–oxygen bond length to the bromine fraction at the corresponding halogen site (Fig. 5). The mutual arrangement of the quasi-equivalent halogen sites suggests the presence of a screw two-fold axis, which is parallel to the [010] axis. This argues for the monoclinic space group $P12_11$. This space group seems to be the most appropriate choice, however, some slight triclinic distortions can occur, so that the triclinic symmetry cannot be eliminated unambiguously.

The similar Cl/Br ordering scheme in the birefringent {100} growth sectors of $Na(ClO_3,BrO_3)$ solid solutions was found by Crundwell et al. [12], who refined 11 crystal structures in the triclinic space group $P1$. Summarizing all the data, one can conclude that the *Hal*11 and *Hal*12 sites (Cl(1) and Cl(3) in the paper [12]) have similar occupancies x_{11} and x_{12} and always contain more Br than the two other sites *Hal*21 and *Hal*22 (Cl(2) and Cl(4) in the paper [12]) with the similar occupancies x_{21} and x_{22}. This scheme allows us to use the averaged (monoclinic) occupancies $x_1 = (x_{11} + x_{12})/2$ and $x_2 = (x_{11} + x_{12}/2)$ instead of the initial triclinic values. In the ideal monoclinic crystal structure these two values are sufficient for the description of ordering. In reality, most crystal structures have additional triclinic distortions, which can easily be described by the degree of triclinicity

Table 4
Atomic coordinates, temperature factors and site occupancies for the samples H1 (upper line) and H2 (lower line); space group $P1$

Site	Occupancy	x	y	z	$U_{eq} \times 100$ (Å^2)
Hal11	$Cl_{0.870(3)}Br_{0.130(3)}$	0.41266(8)	0.41912(8)	0.42129(8)	1.593(9)
	$Cl_{0.730(5)}Br_{0.270(5)}$	0.4098(1)	0.4165(1)	0.4179(1)	1.61(1)
Hal21	$Cl_{0.929(3)}Br_{0.071(3)}$	0.08031(8)	0.58682(8)	0.92220(8)	1.59(1)
	$Cl_{0.775(5)}Br_{0.225(5)}$	0.0823(1)	0.5888(1)	0.9188(1)	1.67(1)
Hal12	$Cl_{0.871(3)}Br_{0.129(3)}$	0.58172(7)	0.91894(7)	0.09024(7)	1.565(9)
	$Cl_{0.713(5)}Br_{0.287(5)}$	0.5831(1)	0.9164(1)	0.0912(1)	1.66(1)
Hal22	$Cl_{0.933(3)}Br_{0.067(3)}$	0.91394(8)	0.08677(8)	0.58880(8)	1.55(1)
	$Cl_{0.788(5)}Br_{0.212(5)}$	0.9116(1)	0.0882(1)	0.5896(1)	1.70(1)
Na1	1	0.0668(2)	0.0731(2)	0.0749(2)	2.43(3)
	1	0.0699(3)	0.0740(3)	0.0741(3)	2.36(4)
Na2	1	0.4282(2)	−0.0661(2)	0.5758(2)	2.34(3)
	1	0.4287(3)	−0.0675(3)	0.5758(3)	2.31(4)
Na3	1	−0.0724(2)	0.5727(2)	0.4366(2)	2.39(3)
	1	−0.0713(3)	0.5736(3)	0.4338(3)	2.31(4)
Na4	1	0.5670(2)	0.4340(2)	−0.0644(2)	2.37(3)
	1	0.5696(3)	0.4322(3)	−0.0665(3)	2.40(4)
O1	1	0.2986(4)	0.5971(4)	0.5107(4)	2.68(5)
	1	0.2996(5)	0.5983(5)	0.5088(5)	2.58(7)
O2	1	0.1944(4)	0.4103(3)	0.0108(4)	2.63(5)
	1	0.1986(5)	0.4088(5)	0.0100(5)	2.64(8)
O3	1	0.6957(4)	0.0970(3)	0.0003(4)	2.61(5)
	1	0.6996(5)	0.0981(5)	−0.0006(5)	2.64(8)
O4	1	0.8005(4)	−0.0892(3)	0.5002(4)	2.67(5)
	1	0.8004(5)	−0.0910(5)	0.4999(5)	2.61(8)
O5	1	0.5022(4)	0.3056(4)	0.5986(3)	2.65(5)
	1	0.5049(5)	0.3025(5)	0.5985(5)	2.66(8)
O6	1	0.0027(4)	0.2009(4)	0.4135(3)	2.72(6)
	1	0.0039(5)	0.2017(5)	0.4103(5)	2.55(7)
O7	1	−0.0076(4)	0.7004(4)	0.0981(3)	2.69(5)
	1	−0.0070(5)	0.7023(5)	0.0982(5)	2.57(7)
O8	1	0.4919(4)	0.8048(4)	−0.0873(3)	2.64(5)
	1	0.4939(5)	0.8027(5)	−0.0905(5)	2.64(8)
O9	1	0.5902(3)	0.5090(4)	0.3077(4)	2.67(5)
	1	0.5941(5)	0.5083(5)	0.3054(5)	2.61(8)
O10	1	0.4042(3)	0.0094(4)	0.2038(4)	2.68(5)
	1	0.4049(5)	0.0085(5)	0.2043(5)	2.61(8)
O11	1	0.0897(3)	−0.0016(4)	0.7034(4)	2.77(6)
	1	0.0934(5)	−0.0029(5)	0.7038(5)	2.61(8)
O12	1	−0.0957(3)	0.4981(4)	0.8076(4)	2.63(5)
	1	−0.0957(5)	0.4977(5)	0.8058(5)	2.61(8)

$U_{eq} = 1/3[U_{11}a^{*2}a^2 + \cdots 2U_{23}b^*c^*bc\cos\alpha]$.

$\xi = (|x_{11} - x_{12}|, |x_{21} - x_{22}|)(\max/x_1 - x_2)$. $\xi = 0$ for a monoclinic crystal with $x_{11} = x_{12}$ and $x_{21} = x_{22}$, and $\xi > 0$ for a triclinic crystal. If $\xi > 1$, the differences between x_{11} and x_{12} (and/or x_{21} and x_{22}) become higher than the differences between x_1 and x_2, so the crystal does not tend to show pseudo-monoclinicity. The degree of triclinicity did not exceed 0.55 for 10 of 13 crystals that permitted us to use the monoclinic occupancies and analyze the halogen ordering over two sites.

The ordering over the *Hal*1 and *Hal*2 sites is described by the degree of ordering $\eta = (x_1 - x_2)/(1 - |1 - x_1 - x_2|)$ or by the intersite distribution coefficient $K_{21} = ((1 - x_1)/x_1)\,(x_2/(1 - x_2))$. The first value is more transparent but the second one should reflect the energetic differences between the sites on the crystal surface. Thus, the ordering state of $Na(ClO_3,BrO_3)$ solid solutions is described by the two variables the first of which shows the most pronounced ordering over the two pairs of sites. This variable can be expressed through the degree of ordering η or through the intersite distribution coefficient K_{12}. The second variable characterizes the differences in occupancies within these pairs and can be expressed as the degree of triclinicity ξ. The degree of ordering varies from 0.1 to 0.5, whereas the degree of triclinicity covers nearly the full range of the different pseudo-monoclinic structures from the structure with $\xi = 0.07$ (deviations from the monoclinic symmetry are very small) to the structure with $\xi = 0.94$ (the pseudo-monoclinicity is hardly to be found)—see Fig. 6. The difference $x_1 - x_2$ (and, consequently, the

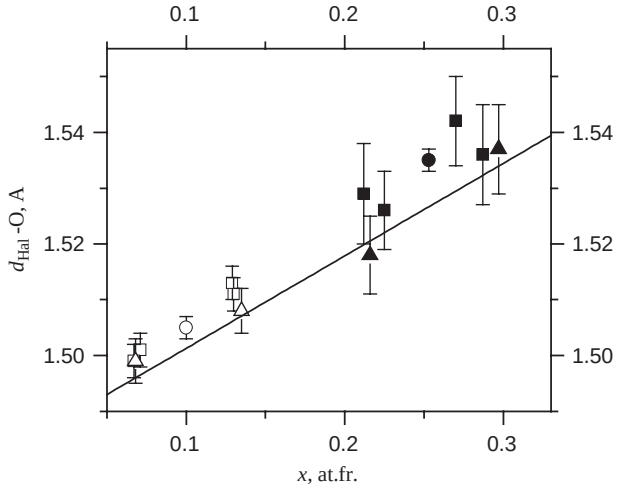

Fig. 5. Average halogen—oxygen bond length as a function of the halogen site occupancies by Br. Open symbols—sample H1, solid symbols—sample H2; circles, triangles and squares correspond to the space groups $P2_13$, $P2_1$ and $P1$, respectively; solid line links the corresponding values for the end members [20,21].

degree of triclinicity) increases as the average composition nears the middle of the isomorphous series and reaches the maximum at $x \approx 0.65$ (Fig. 7a). One remarkable feature consists in the linear correlation between the lattice angle β—90° and the difference $x_1 - x_2$ (Fig. 8). This confirms the accuracy of the structure refinements and supports the applicability of the monoclinic approximation.

3.4. Calculation of the optical indicatrix

We tried to calculate the optical indicatrix for both the samples refined in the monoclinic and triclinic space groups, but failed to get any plausible results for the triclinic crystal structures. The same happened to the attempts of the authors of [12]. However, within the frame of the monoclinic space group the calculated orientation of the optical indicatrix reproduced the observed orientation quite reasonably (Fig. 1). The uncertainty in calculation remains in locating the axis

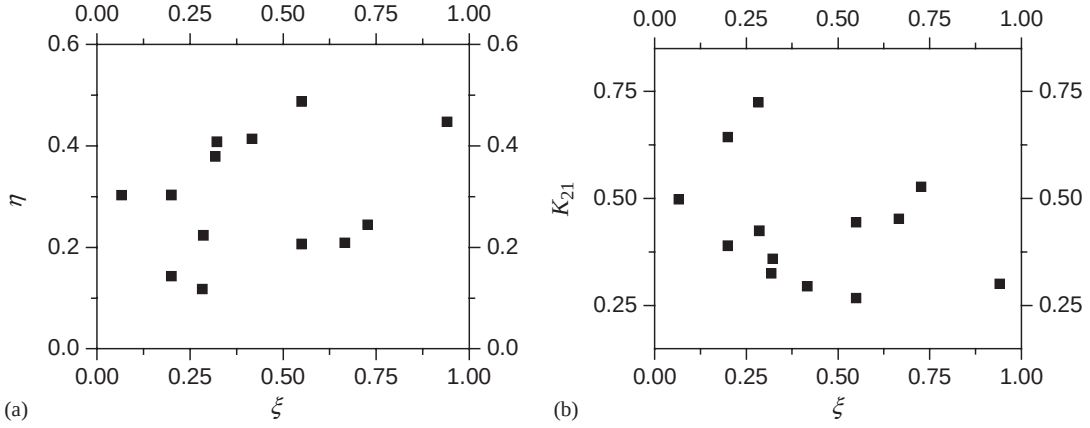

Fig. 6. Ordering over two sites in the monoclinic approximation (degree of ordering η (a) and intersite distribution coefficient K_{21} (b)) vs. triclinic distortions of the crystal structure (degree of triclinicity ξ).

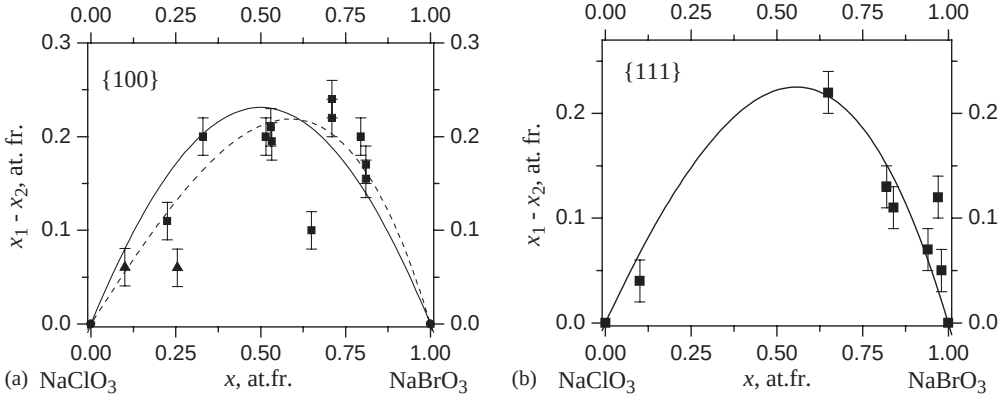

Fig. 7. Occupancy differences between bromine- and chlorine-rich populations of halogen sites for {100} (a) and for {111} and $\{\bar{1}\bar{1}\bar{1}\}$ (b) growth sectors. Triangles—our data, squares—data from [12]. Solid lines were drawn using Eq. (3), dashed line—using Eq. (4) with the values of the distribution coefficient K_{21}, which depend on the average composition x in accordance with Eq. (5).

(n_γ or n_α), which lies in the obtuse angle β. The calculated value of the axial angle $2V = 85$–$87°$ was close to the observed value of nearly 90°. The calculations of birefringence for the samples H1 and H2 gave the values $n_\gamma - n_\alpha = 0.0061$ and 0.0080, respectively, which were by an order of magnitude higher than the observed values of 0.0007 and 0.0010. The discrepancy may be explained by uncertainties in the electronic polarizabilities of atoms. Nonetheless, the calculations agree to some extent with the experimental data and, therefore, halogen ordering can be proposed as the main reason for the anomalous birefringence in $Na(ClO_3, BrO_3)$ solid solutions. However, the following important question has to be clarified: why did the attempts to calculate the optical indicatrix fail for the triclinic space group? It may be assumed that the refinement in the pseudosymmetric triclinic space group $P1$ gives the errors in the atomic coordinates, which are higher than those in the monoclinic space group $P2_1$. These errors do not hinder the crystal structure refinement in converging to low R factors, but they affect the calculations of the optical indicatrix and may heavily distort the results. The same has been observed for the garnets of grossular-andradite solid solutions [5].

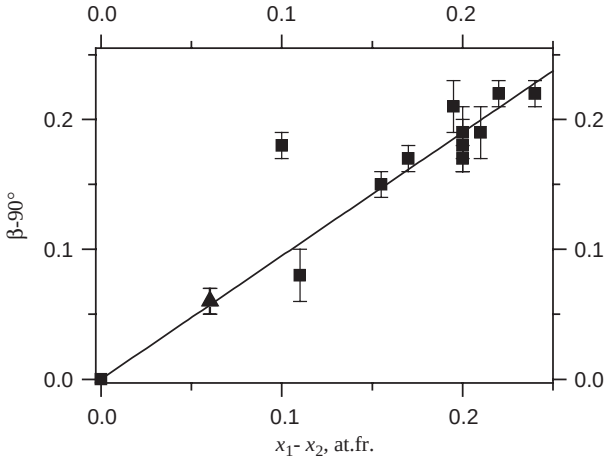

Fig. 8. Lattice constant β as a function of the difference between bromine-rich and bromine-poor populations of halogen sites in the {100} growth sectors. Triangles—our data, squares—data from [12], the case of $\beta = 90°$ corresponds to the ideal cubic crystal structure.

4. Discussion

4.1. Crystal symmetry

The growth dissymmetrization hypothesis presumes the symmetry reduction of a growth sector structure down to the symmetry of the growth front (i.e. to the symmetry of a face or of a step in the cases of normal or tangential growth, respectively). The {100} faces of $Na(ClO_3,BrO_3)$ have the point symmetry 2, and the steps on these faces have the symmetry 1. It means that dissymmetrization should lead to monoclinic symmetry when growing by normal mechanism or to the triclinic one when the growth happens through the step motion along the face. In the former case, the four halogen sites, which were initially equivalent, are divided into two pairs of sites with equal occupancies within each pair. In the latter case, these four sites are occupied differently. This conclusion comes from group theory [7] and is confirmed by the analysis of sets of equivalent positions within the possible space groups.

Let us compare the theoretical distribution of site occupancies with the atomic structure of the growth front. Fig. 9 shows the projection of the crystal structure on the (010) growth face. The chlorate–bromate groups $HalO_3$ form the pyramids with regular triangles of oxygen atoms in their base. These triangles have equal

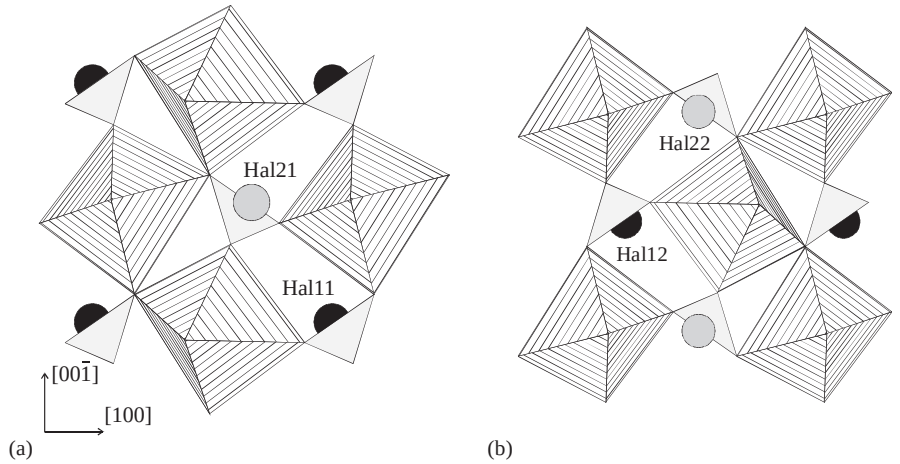

Fig. 9. (010) projections of the triclinic sodium chlorate–bromate structures. (a) $y = (0.5 \pm 0.41)d_{100}$, (b) $y = (0 \pm 0.41)d_{100}$. Hatched polyhedra correspond to NaO_6 octahedra, gray triangles denote the bases of $HalO_3$ pyramids. Halogens are shown by black balls (*Hal*11 and *Hal*12 sites) and gray balls (*Hal*21 and *Hal*22 sites).

slopes to the growth face, but the halogen atoms are situated either above the triangles or below them (the so-called up- and down-positions). When the halogen groups are attached to the crystal structure, the up-positions are more preferable for the larger BrO_3 groups than the down-positions. The geometrical difference is likely to induce growth ordering of the halogens over both the sites and to reduce the crystal symmetry down to the monoclinic space group $P2_1$. In the triclinic space group $P1$ the up- and down-positions correspond to the pairs of sites with similar occupancies (*Hal*11 and *Hal*12 vs. *Hal*21 and *Hal*22 sites). Our experimental data agree completely with the above ordering scheme (Table 4). Growth by step motion provides the differences in the geometrical surroundings for all the four positions giving them the different occupancies and leading to the triclinic space group $P1$.

The $Na(ClO_3,BrO_3)$ crystals are formed by the dislocation-spiral mechanism, i.e. they grow by the tangential motion of the steps along the growth faces (see e.g. [24]). This should result in triclinic symmetry and four different occupancies that is in a good agreement with the experimental data. The pseudo-monoclinic distribution of the occupancies (Table 4) points to the dominant role of the non-equivalence of halogen sites with respect to the growth face or the action of the diffusion relaxation phenomenon [25]. Therefore, all the $Na(ClO_3,BrO_3)$ crystal structures should be considered as triclinic but with a pseudo-monoclinic distribution of halogen occupancies.

It is necessary to note that growth by tangential motion of the steps should provide subsectoral or intrasectoral zoning, so that the single growth sector is divided into few fragments or domains with very similar triclinic crystal structures but with different orientations with respect to the common coordinate frame. These domains are frequently observed under a polarizing microscope, however, it is difficult to detect them using X-ray diffraction method. Firstly, their sizes are large (up to few mm) and the samples usually contain only one domain. Moreover, the crystal structures of different domains are very similar (even taking their different orientations into account) and domains superimposing will cause no additional reflections, but only redistribution of intensities and broadening of reflections.

Crundwell et al. [12] have indexed the set of eleven $Na(ClO_3,BrO_3)$ crystals and have found fundamentally different orientation of [010] axis with respect to the growth front: it lied in the growth plane, i.e. perpendicular to the growth direction. This orientation contradicts the monoclinic symmetry and leaves the only possible space group $P1$. The inconsistency looks quite incomprehensible keeping in mind the similarity of the growth conditions, optical properties, lattice constants, and Cl/Br distribution over the halogen sites.

4.2. Effect of crystal composition

The effect of crystal composition on growth ordering has been already considered in [2]. Let us discuss it in more detail. Let two different sorts of atoms A and B occupy two different positions: 1 and 2. Since the crystal is in equilibrium (or close to equilibrium) with the aqueous solution, an equilibrium distribution coefficient of each site in the crystal surface with respect to the solution is expressed as $K_i = (x_i/(1-x_i))\,((1-y)/y)$ [26,27]. Here, x_i is a molar fraction of atoms B in the ith site ($i = 1, 2$), and $y = B/(A+B)$ is a molar fraction of the atoms B in the salt part of the aqueous solution. The relation between these coefficients defines the intersite distribution coefficient as

$$K_{21} = \frac{K_2}{K_1} = \frac{1-x_1}{x_1}\frac{x_2}{1-x_2}. \tag{1}$$

For the sake of definiteness let us assume that $x_1 > x_2$ and, consequently, $K_{21} < 1$. The value of K_{21} is unknown a priori; however, it should be independent of the average crystal composition x for nearly ideal solid solutions (see e.g. [26,27]). Let the multiplicities of the sites 1 and 2 be equal to n_1 and n_2, respectively. The occupancies of these sites can be expressed through the average composition $x = (n_1x_1 + n_2x_2)/(n_1+n_2)$ and through the difference (in) $\delta = (x_1 - x_2)/(n_1+n_2)$:

$$\begin{aligned} x_1 &= x + n_2\delta, \\ x_2 &= x - n_1\delta. \end{aligned} \tag{2}$$

Substitution of Eq. (2) into Eq. (1) defines the quadratic equation with respect to δ. One of the two solutions expresses the effect of the average composition x on the difference $x_1 - x_2$.

$$x_1 - x_2 = \frac{n_1+n_2}{2n_1n_2}\left[x(n_2-n_1) + \frac{K_{21}n_2 + n_1}{1-K_{21}} - \sqrt{\left(x(n_2-n_1) + \frac{K_{21}n_2+n_1}{1-K_{21}}\right)^2 - 4x(1-x)n_1n_2}\right]. \tag{3}$$

This difference equals zero for the end members and has a maximum in the middle of the series. When $n_1 = n_2$, the function (3) is symmetric with respect to $x = 0.5$ and tends to be a parabola as K_{21} nears 1:

$$x_1 - x_2 \approx \frac{2(1-K_{21})}{1+K_{21}}x(1-x). \tag{4}$$

For $K_{21} \ll 1$ the curve has a quasi-parabolic shape with two approximately linear segments in the vicinity of the end members and a smooth maximum between these segments. When $n_1 > n_2$ and $x_1 - x_2 > 0$, the maximum is shifted toward the end member B. Similar dependence is expected for the anomalous birefringence $n_\gamma - n_\alpha$, since this value should be roughly proportional to the difference $x_1 - x_2$.

In the crystal structure of $Na(ClO_3,BrO_3)$ there are four different halogen sites. Assuming the pseudo-monoclinic Cl/Br distribution in the {100} growth sectors, these sites are grouped into two populations. Each of them contains two sites, i.e. $n_1 = n_2 = 2$. The distribution of sites follows the symmetric quasi-parabolic dependence of $x_1 - x_2$ on the average composition x. In reality (Fig. 7a) one can see an asymmetric parabola-like curve with the maximum at $x \approx 0.65$. A very similar dependence is obtained by plotting $n_\gamma - n_\alpha$ vs. average composition x (Fig. 2). Although the deviations from the theoretical curves are not significant, they are distinct and do not seem to be artifacts. The possible reason for the deviations consists in the inapplicability of the two-site approximation since the degree of triclinicity can be high, especially for the bromine-rich solid solutions. In this case, the averaged difference $x_1 - x_2$ loses its physical meaning, and the intersite Cl/Br distribution should be described by two or even three different independent distribution coefficients.

The further investigation showed that the value of intersite distribution coefficient K_{21} changed along the isomorphous series (Fig. 10). The most part (11 of 13) of the values of K_{21} calculated from the refinements of the occupancies lies close to the straight line approximated by the formula:

$$K_{21} = 0.56 - 0.31x. \quad (5)$$

Taking Eq. (5) into account, Eq. (4) perfectly fits the experimental data (Figs. 2 and 7a).

The {111} and $\{\bar{1}\bar{1}\bar{1}\}$ growth sectors are characterized by division of the four halogen sites into two populations [12]. The first of them includes the special site on the three-fold axis ($n_2 = 1$). The second population consists of the three equally occupied sites ($n_1 = 3$) generated by a three-fold axis. Consequently, the normal growth mechanism should lead to the trigonal space group $R3$, which was found to match the experimental data in the best way. In this case the crystal should be optically uniaxial with the optical axis directed normally to the growth face. In reality, these growth sectors show slight biaxiality with the axial angle $2V = 10-15°$. Biaxiality argues for slight triclinic distortions, which are out of the detection limit of the single crystal structure analysis. The distortions are most probably related to the growth by tangential step motion. Along with the data on the crystal symmetry and optical anomalies, the growth ordering hypothesis is also confirmed by the effect of crystal composition on the Cl/Br ordering (Fig. 7b). Eq. (3) gave a rather good approximation of the dependence of $x_1 - x_2$ on the average composition x. Data on $x_1 - x_2$ were calculated from the refined occupancies of the halogen sites obtained by Crundwell et al. [12].

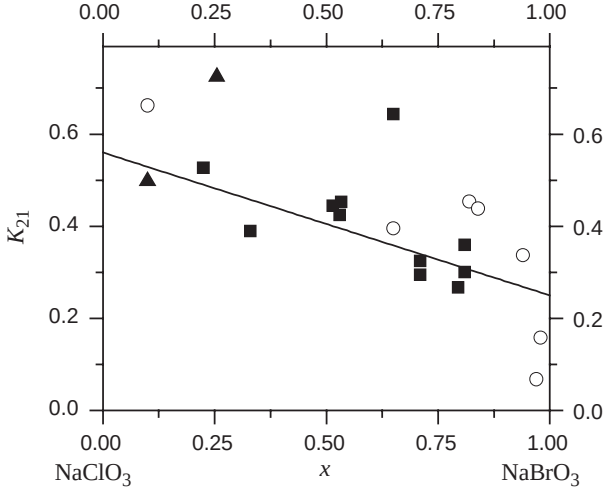

Fig. 10. Intersite distribution coefficient as a function of average composition for {100} growth sector (solid symbols) and {111} and $\{\bar{1}\bar{1}\bar{1}\}$ growth sectors (open symbols). Triangles—our data, squares and circles—data from [12].

5. Conclusion

Generalizing our experimental data on the real structure and the optical anomalies and the relevant data available in the literature [11,12], we confirm the validity of the kinetic ordering mechanism (the growth dissymmetrization) in the case of sodium chlorate–sodium bromate solid solutions.

The $Na(ClO_3,BrO_3)$ solid solutions display partial ordering of the halate groups. In the growth sectors of cube {100}, the four halogen sites, which were initially identical in the ideal cubic space group $P2_13$, are divided into two pairs of sites. Site occupancies differ significantly between these pairs, but within the pairs they are closer to each other. If the differences within the pairs were negligible, the crystal structure would be successfully described by the monoclinic space group $P2_1$. When the differences become more or less significant, the symmetry reduces to the triclinic space group $P1$. In reality, most $Na(ClO_3,BrO_3)$ mixed crystals are triclinic (pseudo-monoclinic) with a different degree of monoclinicity.

The halate ordering is responsible for the anomalous birefringence observed in the crystals of $Na(ClO_3,BrO_3)$ solid solutions. This conclusion is confirmed by the calculations of the optical indicatrix using point-dipole approximation.

The orientations of the above-mentioned two pairs of halate groups with respect to the {100} growth face show distinct geometrical non-equivalence. The differences within these pairs exist with respect to the growth steps only. The geometrical non-equivalence serves as a basis for the anion ordering through the growth dissymmetrization mechanism. Consequently, normal

growth provides the differences between pairs of sites and leads to the monoclinic symmetry, whereas tangential step motion provides the differences within the pairs and leads to triclinic symmetry.

However, it should be, repeated that the monoclinic direction with respect to the growth direction is different from that in [12]. This difference leads to a rather different interpretation of the results obtained.

The effect of the crystal composition on the anomalous birefringence and ClO_3/BrO_3 distribution for both the cubic and tetrahedral growth sectors is in line with the predicted theoretical behavior.

Acknowledgments

The work was partly supported by RFBR (project 02-05-65279). The authors are grateful to T.I. Ivanova for help in preparation of the manuscript.

References

[1] L.I. Tsinober, M.I. Samoilovich, in: B.K. Wainshtein, A.A. Chernov (Eds.), Problems of the modern crystallography, Nauka, Moscow, 1975, pp. 207–218 (in Russian).
[2] A.G. Shtukenberg, Yu.O. Punin, V.N. Soloviev, Mineral. Mag. 64 (2000) 837–845.
[3] A.G. Shtukenberg, Yu.O. Punin, E. Haegele, H. Klapper, Phys. Chem. Minerals. 28 (2001) 665–674.
[4] M. Wildner, M. Andrut, Am. Mineral. 86 (2001) 1231–1251.
[5] A.G. Shtukenberg, D.Yu. Popov, Yu.O. Punin, Mineral. Mag. 66 (2002) 275–286.
[6] M. Akizuki, M.C. Hampar, J. Zussman, Mineral. Mag. 43 (1979) 237–241.
[7] G.R. Bulka, V.M. Vinokurov, N.M. Nizamutdinow, N.M. Hasanova, Phys. Chem. Minerals. 6 (1980) 283–293.
[8] Y. Takéuchi, N. Haga, S. Umizu, G. Sato, Z. Kristallog. 158 (1982) 53–99.
[9] A.G. Shtukenberg, Yu.O. Punin, O.V. Frank-Kamenetskaya, O.G. Kovalev, P.B. Sokolov, Mineral. Mag. 65 (2001) 463–477.
[10] A.G. Shtukenberg, Yu.O. Punin, O.G. Kovalev, Crystallogr. Rep. 43 (1998) 465–468.
[11] P.S.H. Gopalan, M.L. Peterson, G. Crundwell, B. Kahr, J. Am. Chem. Soc. 115 (1993) 3366–3367.
[12] G. Crundwell, P. Gopalan, A. Bakulin, M.L. Peterson, B. Kahr, Acta Crystallogr. Sect. B 53 (1997) 189–202.
[13] A.N. Winchell, H. Winchell, The Microscopic Character of Artificial Inorganic Solid Substances: Optical Properties of Artificial Minerals, Academic Press, New York and London, 1964.
[14] L.G. Akselrud, Yu.N. Grin, P.Yu. Zavalii, V.K. Pecharsky, V.S. Fundamensky, Coll. Abstr. XII ECM 3 (1989) 155.
[15] D.T. Cromer, J.T. Waber, International Tables for X-ray Crystallography, Vol. IV, Kynoch, Birmingham, UK, 1974.
[16] D. Pohl, Acta Crystallogr. Sect. A 34 (1978) 574–578.
[17] R.N. Abbott Jr., Am. Mineral. 78 (1993) 952–956.
[18] R.N. Abbott Jr., Can. Mineral. 34 (1996) 595–603.
[19] S.S. Batsanov, Structural refractometry, Visshaya shkola, Moscow, 1976 (in Russian).
[20] S.C. Abrahams, J.L. Bernstein, Acta Crystallogr. Sect. B 33 (1977) 3601–3604.
[21] D.H. Templeton, L.K. Templeton, Acta Crystallogr. Sect. A 41 (1985) 133–142.
[22] F. Mussard, S. Goldsztaub, J. Cryst. Growth 13/14 (1972) 445–448.
[23] M. Matsunaka, M. Kitamura, I. Sunagawa, J. Cryst. Growth 48 (1980) 425–434.
[24] R. Ristic, J.N. Sherwood, K. Wojciechowski, J. Phys. Chem. 97 (1993) 10774–10782.
[25] A.A. Chernov, Modern crystallography, in: Crystal Growth, Vol. III, Springer, Berlin, 1984.
[26] C. Balarew, Z. Kristallogr. 181 (1987) 35–82.
[27] P.Ya. Azimov, A.G. Shtukenberg, Russian J. Inorg. Chem. 34 (2000) 1302–1309.